Demonstration of Cascaded Modulator-Chicane Microbunching of a Relativistic Electron Beam

N. Sudar, P. Musumeci, I. Gadjev, Y. Sakai, S. Fabbri, M. Polyanskiy, I. Pogorelsky, M. Fedurin, C. Swinson, K. Kusche, M. Babzien, and M. Palmer

Phys. Rev. Lett. **120**, 114802 — Published 15 March 2018

DOI: 10.1103/PhysRevLett.120.114802

Demonstration of cascaded modulator-chicane micro-bunching of a relativistic electron beam

N. Sudar, P. Musumeci, I. Gadjev, Y. Sakai, S. Fabbri
Particle Beam Physics Laboratory,
Department of Physics and Astronomy University of California Los Angeles
Los Angeles, California 90095, USA

M. Polyanskiy, I. Pogorelsky, M. Fedurin, C. Swinson, K. Kusche, M. Babzien, M. Palmer
Accelerator Test Facility Brookhaven National Laboratory
Upton, New York 11973, USA
(Dated: November 7, 2017)

We present results of an experiment showing the first successful demonstration of a cascaded micro-bunching scheme. Two modulator-chicane pre-bunchers arranged in series and a high power mid-IR laser seed are used to modulate a 52 MeV electron beam into a train of sharp microbunches phase-locked to the external drive laser. This configuration is shown to greatly improve matching of the beam into the small longitudinal phase space acceptance of short-wavelength accelerators. We demonstrate trapping of nearly all (96 %) of the electrons in a strongly-tapered inverse free electron laser (IFEL) accelerator, with an order-of-magnitude reduction in injection losses compared to the classical single buncher scheme. These results represent a critical advance in laser-based longitudinal phase space manipulations and find application both in high gradient advanced acceleration as well as in high peak and average power coherent radiation sources.

Progress in the production of high brightness electron beams has provided the scientific community with a wide variety of tools for measuring phenomena at unprecedented spatial and temporal scales, making use of the short wavelength radiation generated by these beams or using the electrons as probe particles directly [1, 2]. Enhancing the capabilities of these investigative tools has become an active area of research aimed at improving the peak and average brightness of the e-beam and the generated radiation, better controlling the spectral-temporal characteristics of the radiation, and decreasing the footprint of these devices using advanced accelerator techniques [3].

All of these schemes demand precise control of the electron beam phase space at optical scales. This is important in the field of high gradient laser-driven accelerators, which includes dielectric accelerators [4] or inverse free-electron lasers (IFEL) [5] among others. In order for these devices to ever be considered a valid alternative to conventional RF-based machines, it is critical to develop new concepts for matching the beam to their extremely small phase space acceptances, increasing their efficiency and minimizing the injection losses [6].

In IFELs, for example, electrons can gain significant energy from a laser driver when interacting resonantly in an undulator field. Only particles injected near the initial resonant energy and phase can be stably accelerated by the ponderomotive potential [7]. To extend the interaction over a long distance, the undulator parameters are tapered to maintain resonance for the particles trapped in the bucket gaining energy at a chosen accelerating resonant phase. Using well-matched input beams can significantly decrease particle losses and improve the system performances [8, 9].

Optical-scale longitudinal phase space control of relativistic beams is usually based on combining the sinusoidal energy modulation imparted by a laser in an undulator magnet, with a dispersive element such as a magnetic chicane or a simple drift. Modulator-chicane pre-bunching has been used to great effect, both for coherent radiation generation and in high gradient laser-driven acceleration [10–14]. Nevertheless, the inherent limitations of this scheme (non linear sinusoidal dependence of the energy modulation) strongly limit the quality of the bunching that can be achieved, and are ultimately responsible for the large losses in injection trapping in laser accelerators as well as in a reduced energy efficiency of beam based coherent radiation sources. Adding several of these modulator-chicane elements in series with varying modulation amplitudes, laser wavelengths and dispersive strengths allows for tailoring of the energy and density distributions, thus gaining greater control of the electron beam peak current, coherent form factor, and output energy spread [15–19].

In this letter, we present the results of an experiment successfully demonstrating a novel bunching scheme whereby using two modulator chicane pre-bunchers in series we are able to produce a sequence of sharp spikes in the electron beam density profile, periodically spaced at the wavelength of a mid-IR seed laser. Subsequently injecting these micro-bunches into the periodic stable ponderomotive potential of a strongly tapered undulator interaction in the accelerating configuration [20, 21], driven by the same seed laser pulse, we are able to trap and accelerate nearly all (96%) of the injected 52 MeV electron beam, with 78% of the particles reaching the final design

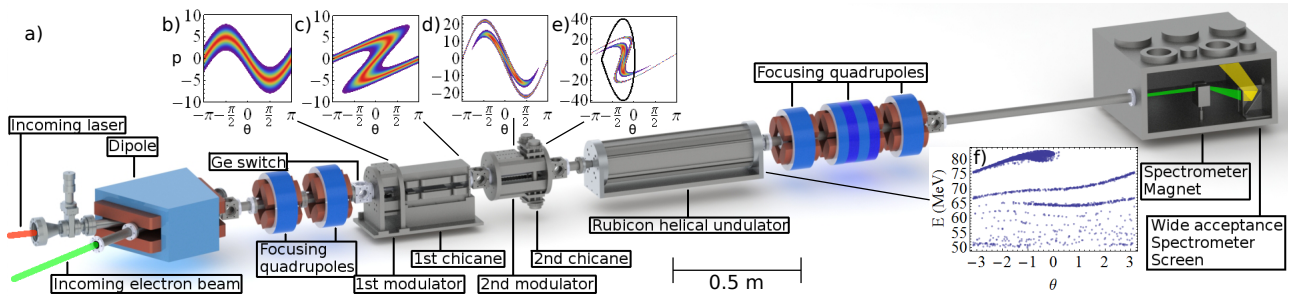

FIG. 1. a) Experiment beamline layout. b)-e) Electron beam phase space after first modulator, first chicane, second modulator, second chicane from analytical model. f) Phase space after IFEL acceleration

energy of 82 MeV over the 54 cm undulator length with an RMS energy spread of 1%.

In order to understand quantitatively the benefits of the cascaded buncher configuration we can start from the equations describing the energy exchange between an electromagnetic wave and a relativistic electron beam copropagating in an undulator field (Eq. 1,2) [22, 23].

$$\frac{d\gamma^2}{dz} = -kK_lKJJ\sin(\theta) \tag{1}$$

$$\frac{d\theta}{dz} = k_w - \frac{k(1+\frac{K^2}{2})}{2\gamma^2} = 0 \rightarrow \gamma_r^2 = \frac{k(1+\frac{K^2}{2})}{2k_w} \tag{2}$$

where k_w and k are the undulator and laser wavenumbers, $K = \frac{eB_0}{k_w m_e c}$ and $K_l = \frac{eE_0}{km_e c^2}$ are the undulator and laser vector potentials, $JJ = J_0(\frac{K^2}{4+2K^2}) - J_1(\frac{K^2}{4+2K^2})$, γ and θ represent the particle Lorentz factor and phase respectively and γ_r is defined as the resonant energy, with both expressions applying to a planar undulator geometry.

Over a short distance we can ignore the phase evolution resulting in a sinusoidal energy modulation with a modulation amplitude of $\Delta\gamma \sim -kK_lKJJL_u/2\gamma_r$, where L_u is the effective length of the interaction. Transformation of the scaled phase space variables, $p \equiv \frac{\gamma-\gamma_r}{\sigma_\gamma}$ and $\theta \equiv kz$, where σ_γ is the electron beam initial energy spread, gives $p' = p + A\sin(\theta)$ and $\theta' = \theta$, where $A = \Delta\gamma/\sigma_\gamma$.

This energy modulation can be transformed into a density modulation using a dispersive element such as a 4-dipole magnetic chicane, transforming the phase space variables to, $p'' = p'$ and $\theta'' = \theta' + B[p + A\sin(\theta')]$, where $B \equiv \frac{R_{56}k\sigma_\gamma}{\gamma_r}$ with R_{56} being the dispersive strength of the chicane. Choosing $B \sim \frac{\pi}{2A}$ will produce a series of density microbunches resulting from the rotation of the distribution in longitudinal phase space.

Adding a modulator chicane module before the final pre-buncher serves to greatly increase the number of particles in the linear region of the sinusoidal energy modulation, as shown in Figure 1d [24–26]. This scheme can be described defining the modulation amplitudes and scaled dispersive strengths, in order, as A_1, B_1, A_2 and B_2. The first modulator imparts a small sinusoidal energy modulation with amplitude A_1, Fig. 1b. The first chicane over-compresses this modulation, maximizing the number of particles between $-\frac{\pi}{2} < \theta < \frac{\pi}{2}$, with $B_1 \sim \frac{\pi}{A_1}$, Fig. 1c. The second modulator imparts a final sinusoidal energy modulation, now with a much larger fraction of particles in the linear region, Fig. 1d. The second chicane rotates this energy modulation into density modulation with $B_2 \sim \frac{\pi}{2A_2}$, Fig. 1e. Fig. 2a shows polynomial fits to the values of A_1, B_1, and B_2 which optimize the scheme as a function of the final modulation amplitude A_2. For large A_2, the optimal relative dispersion strengths B_1 and B_2 converge to the qualitative estimates discussed above. The figure of merit for the manipulation depends on the final application. For radiation generation the coherent form factor, $|b|^2 = |< e^{i\theta} >|^2$ is often used. For advanced accelerators, one needs to maximize the fraction of particles trapped, f_T, into a ponderomotive bucket. In this case, assuming the same laser beam drives the tapered undulator interaction with a resonant phase θ_r, the energy acceptance of the accelerator is $A_b \propto \sqrt{K_l(\cos[\theta_r] + (\frac{\pi}{2} + \theta_r)\sin[\theta_r])}$.

The cascaded pre-bunching scheme in theory shows a factor of 2 increase in the coherent form factor, $|b|^2$ (i.e. from 0.32 to 0.7) and an order of magnitude decrease in the estimated injection losses (i.e. from 20% to 2 %) compared to the single pre-buncher (see Fig. 2b). The points in Fig. 2 correspond to the experimental parameters in our setup. For initial trapping in the pondero-

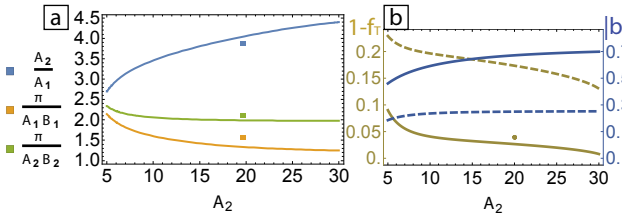

FIG. 2. a) Optimal double buncher parameter values maximizing trapping. b) Double buncher and single buncher (dashed) injection losses (yellow) and coherent form factor (blue). Experimental values corresponding to $A_2 = 20$ are also shown as points in the graphs.

motive potential of the Rubicon IFEL, with $\theta_r = -\frac{\pi}{4}$ we have $A_2 = 20$ and $A_b = 40$, and the estimated trapped fraction in the double-buncher case is $\sim 96\%$.

Figure 1a shows a schematic of the beamline at Brookhaven National Laboratory Accelerator Test Facility (ATF) with both modulator chicane pre-bunchers and the Rubicon helical undulator. Experimental parameters are summarized in Table 1. A several picosecond long 10.3 μm wavelength high power pulse from a CO_2 laser is used to drive the interactions in both modulator chicane modules and the IFEL. The laser pulse is focused using a 4 m focal length NaCL lens to a 1.06 mm waist at the center of the undulator. After the interaction the laser intensity decreases due to diffraction and, after passing through the gap of the dipole spectrometer, is absorbed by a beam dump. Including transport losses the laser power delivered to the IFEL fluctuates between 70-100GW.

The electron beam is coaligned to the laser propagation axis after passing through a dipole and then focused by a quadrupole doublet to a cross section which remains much smaller than the laser along the entire interaction region. Picosecond scale timing between laser and electron beam arrival time is achieved first utilizing electron-beam controlled transmission of the mid-IR pulse in a semiconductor (Ge) slab [27] and then optimized by maximizing the energy modulation on the electron spectrometer. The laser pulse is longer than the electron bunch and the system is stable under timing jitter of $\sim$1 ps. Both modulator chicane modules could be removed and inserted on the beamline without alignment errors, allowing for separate optimization of each component.

The first modulator consists of a half period planar Halbach undulator with period 7 cm. This is followed by an electromagnetic chicane consisting of 4 dipole electromagnets of length 3 cm separated by 3 cm drifts with a field of 2.25 mT/A over the range of 0-150 A, corresponding to $R_{56} = 0 - 900\mu$. The second modulator consists of a single period planar Halbach undulator with period 5 cm. This is followed by a variable gap permanent magnet chicane composed of 4 dipole magnets of length 12.5 mm whose gap can be adjusted from a minimum of 15.9 mm to a maximum of 22 mm and are interspaced by drifts of 12.5 mm, corresponding to $R_{56} = 40 - 90\mu$m, Figure 3. The Rubicon helical undulator is made up of two 11 period Halbach undulators, oriented perpendicularly and shifted in phase by $\pi/2$ with period increasing from 4.04 cm to 5.97 cm. The resonant energy of the undulator is tuned from 52 MeV at the entrance to a final energy of 82 MeV. The laser pulse is circularly polarized to drive the helical undulator interaction. The use of planar modulators for both pre-bunchers, combined with diffraction effects, results in a modulation to bucket height ratio of $\frac{A_b}{A_2} = 2$.

The adjustable field of both chicanes allows for both tuning of the optimal B_1 and B_2 and precise control of the relative injection phase between the laser and the electron microbunches at both the second modulator and the undulator entrance. In the experiment we first optimize B_2, inserting the downstream modulator chicane module, and scanning over the variable chicane gap, Figure 4a. On the electron spectrometer, we observe two peaks in the fraction of trapped particles in the IFEL corresponding to phase slippages $S = 6\pi + \pi/4$ and $S = 8\pi + \pi/4$, corresponding to injection at the expected resonant phase, $-\pi/4$, with $B \sim \frac{2\sigma_\gamma S}{\gamma_r}$. Setting the downstream chicane at the larger delay, we insert the upstream module and optimize B_1, varying the current in its chicane, Figure 4b. We observe two peaks in the fraction of particles trapped corresponding to phase delays near 40π and 42π, corresponding to injection at 0 phase offset at the entrance of the second buncher.

The interaction is simulated with General Particle Tracer (GPT) [28] using measured electron beam parameters and 3D field maps from the magnetostatic solver Radia [29], which agree with Hall probe measurements of the undulator and both pre-bunchers. Laser parameters used in simulations are taken from measurements on the unamplified pulse, indicating a nearly ideal trans-

TABLE I. Parameters for the Rubicon experiment.

Parameter	Value
Initial electron beam energy	52 MeV
Initial beam energy spread ($\frac{\Delta\gamma}{\gamma}$)	0.0015
electron beam emittance ($\epsilon_{x,y}$)	2.5 mm-mrad
electron beam waist ($\sigma*_{x,y}$)	80μm
electron beam length (σ_z)	1 ps
electron beam charge	80 pC
Laser wavelength	10.3μm
Rayleigh range	0.34 m
Laser waist	1.06 mm
Waist position (undulator entrance @ z=0)	0.16 m
Laser Power	75 GW

Parameter	1^{st} Buncher	2^{nd} Buncher	Rubicon
K	2.02	2.56	2.07 - 2.80
K_l	0.0035	0.006	0.017
λ_w	0.07m	0.05m	0.04-0.06m
Effective length L_u	0.04m	0.075m	0.5475m
Modulation(A,ΔE)	5.1, 0.4 MeV	20, 1.6 MeV	–
Dispersion(B,R_{56})	0.44, 480 μm	0.075, 80 μm	–

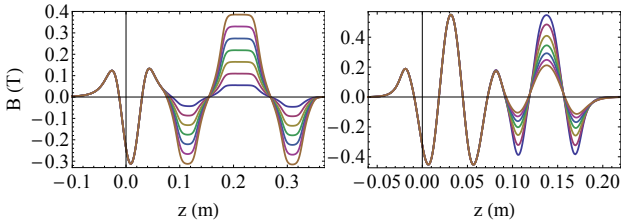

FIG. 3. Hall probe measurements of upstream (left) and downstream (right) bunchers varying chicane current and chicane gap.

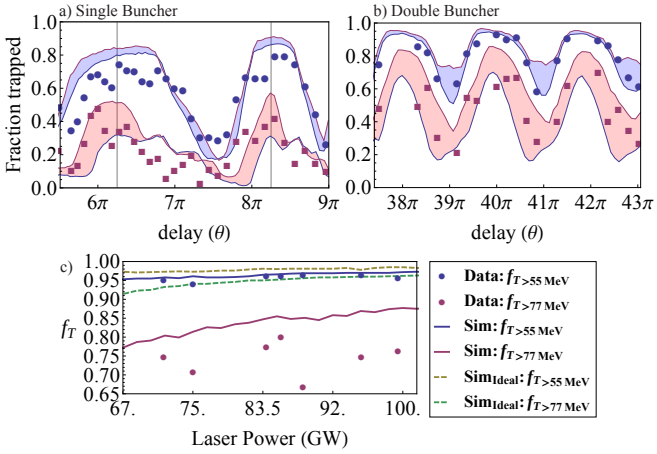

FIG. 4. Single shot experimental data (dots) showing $f_T >$ 55MeV (Blue) and $f_T >$ 77MeV (red) varying downstream pre-buncher chicane gap (a) and upstream pre-buncher chicane current (b) compared with GPT simulations with lower and upper lines corresponding to 70 GW and 100 GW laser power respectively. c) Single shot experimental data after double buncher optimization (dots) showing $f_T >$ 55MeV (blue) and $f_T >$ 77MeV (red) vs. laser power compared with GPT simulation with experimental and ideal parameters.

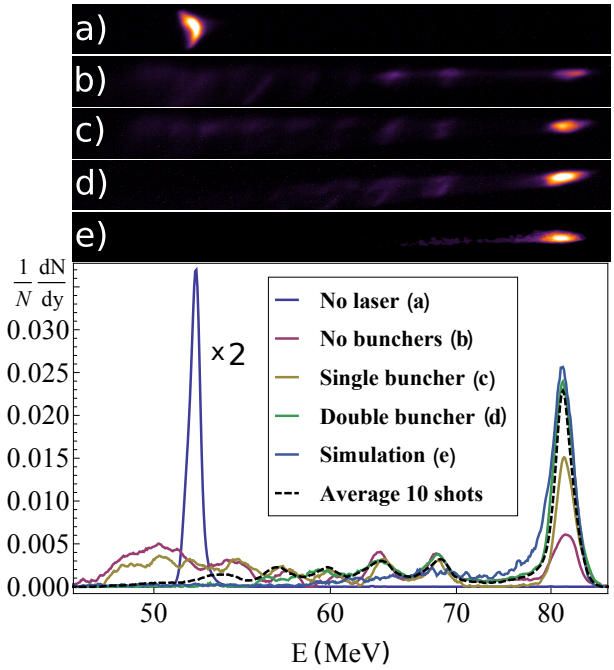

FIG. 5. a)-e) Single shot Raw spectrometer images with no laser seed, no bunchers, downstream buncher only, both bunchers and GPT simulation. (Bottom) Single shot projections showing electron beam energy distribution $\frac{1}{N}\frac{dN}{dy}$ vs. E and 10 shot average of double buncher spectrum.

verse gaussian profile with $M^2 = 1.1$. Simulations and data show close agreement for initial trapping which we defined here as the fraction of particles above E > 55 MeV, and acceleration to the final energy, E > 77 MeV. Simulations show $|b|^2$=0.67 at the entrance of the IFEL. Detrapping throughout the IFEL accelerator can be attributed to undulator alignment and trajectory errors as well as to non ideal electron beam and laser focusing. It is important to note that for the single buncher case, only slightly more than half of the initially trapped particles are accelerated to the final energy, compared to $\sim$ 90% for the double buncher (blue and red curves in Fig. 4a,b). This increase in stability is ascribed to the better matching of the input beam to the resonant ponderomotive bucket when using the cascaded buncher scheme.

Figure 4c reports the fraction of particles trapped as a function of the fluctuating input laser power after optimization of both prebuncher dispersion and delays, showing a peak of 96% of the particles accelerated past 55 MeV and up to 78% accelerated to the final energy, in agreement with simulations using experimental parameters. When simulating the interaction in GPT using ideal laser and electron beam parameters (dashed lines), we observe that nearly all particles accelerated past 55 MeV are accelerated to the final energy, validating our operational estimate for initial trapping as the fraction of particles accelerated above 55 MeV.

In Fig. 5 we show energy spectrometer images taken with no laser, no bunchers installed, the downstream buncher installed, both bunchers installed and their relative distribution projections $\frac{1}{N_{tot}}\frac{dN}{dy}$ normalized so that the integral under the curves is 1, with all spectra taken from the same experimental run with a nominal 75 GW laser seed power. The average over 10 consecutive shots is also shown, demonstrating the stability and reproducibility of this acceleration. The energy spread of the accelerated beam is $\sim$ 1% set by the amplitude of the ponderomotive bucket at the exit of the undulator. The normalized emittance is conserved through the acceleration and was measured in the non-bend plane of the spectrometer using the quadrupole scan technique, to be $2.6 \pm 0.2\mu$m, within the experimental uncertainty, equal to the input value.

In conclusion, the cascaded pre-buncher Rubicon experiment demonstrated initial trapping of 96% of a 52 MeV electron beam with up to 78% of the electron beam reaching the final energy of 82 MeV, decreasing the injection losses by an order of magnitude compared to the single buncher case. These results agree well with both simulations and analytical estimates. This experiment took advantage of the favorable parameters of the CO_2 laser, characterized by long pulse lengths and Joule-level energies, allowing use of a single laser pulse to drive the entire interaction with negligible effects from the electron beam slippage from the modulator chicane elements. The long wavelength of the CO_2 laser also allows for increased stability and phase space acceptance. Scaling this scheme to higher energy electron beams and shorter wavelength

laser seeds, which typically exhibit shorter pulse lengths, may require particular care in controlling the timing jitter, relative slippage between electron beam and radiation and phase-locking between the different stages. The use of separate laser pulses to drive each modulator chicane might offer a greater range of tunability between the modulation and dispersion strengths allowing for a large variety of schemes to be investigated.

Successful demonstration of this scheme not only increases the performance of laser based advanced accelerators and their applications, but also encourages exploration into other areas where cascaded pre-bunching can prove useful. This includes schemes where cascaded pre-bunching could be employed to increase the efficiency of a strongly tapered FEL, to increase the electron beam peak current in enhanced self amplified spontaneous emission schemes in an FEL, or to excite resonances in dielectric structures [30–33].

This work was partially supported by DOE grant No. DE-SC0009914, U.S. DHS DNDO under Contract No. 2014-DN-077-ARI084-01 and the DOE SCGSR program. The authors would also like to thank Gerard Andonian for useful comments, Phuc Hoang and Ryan Roussel.

[1] C. Bostedt et al., Rev. Mod. Phys. **88**, 015007 (2016)
[2] A.H. Zewail, Annu Rev. Phys. Chem. **57**, 65 (2006)
[3] E. Hemsing, G. Stupakov, D. Xiang, A. Zholents, Rev. Mod. Phys. **86**, 897 (2014)
[4] R.J. England et al., Rev. Mod. Phys. **86**, 1337 (2014)
[5] J.P. Duris, P. Musumeci, R.K. Li, Phys. Rev. ST Accel. Beams **15**, 061301 (2012)
[6] S. Steinke et al., Nature **530**, 190-193 (2016)
[7] N. M. Kroll, P.L. Morton, M. N. Rosenbluth, IEEE Journ. of Quantum Electronics **17**, 1436 (1981)
[8] J. P. Duris, et al., Nat. Commun. **5**, 4928 (2014)
[9] J. T. Moody, S. G. Anderson, G. Anderson, S. Betts, S. Fisher, A. Tremaine, and P. Musumeci Phys. Rev. Accel. Beams 19, 021305 (2016)
[10] L.H. Yu et al., Phys. Rev. Lett. **91** 074801 (2003)
[11] W.D. Kimura et al., Phys. Rev. Lett. **86** 4041 (2001)
[12] C. Sears et al., Phys. Rev. ST Accel. Beams **11** 101301 (2008)
[13] N. Sudar et al., Phys. Rev. Lett. **117** 174801 (2016)
[14] I. Gadjev et al., arXiv: 1711.00974
[15] G. Stupakov, Phys. Rev. Lett. **102** 074801 (2009)
[16] A.A. Zholents, Phys. Rev. ST Accel. Beams **8** 040701 (2005)
[17] E. Kur et al., New Journal of Physics **13** 063012 (2011)
[18] G. Andonian et al., Phys. Rev. ST Accel. Beams **14** 072802 (2011)
[19] E. Hemsing et al., Phys. Rev. Lett. **102** 174801 (2009)
[20] R.B. Palmer, J. Appl. Phys. **43**, 3014 (1972)
[21] E. D. Courant, C. Pellegrini, W. Zakowicz, Phys. Rev. A **32**, 2813 (1985)
[22] J.M.J. Madey, H. A. Schwettman, W.M. Fairbank. IEEE Trans. Nucl. Sci. **NS-20**, 980 (1973)
[23] R. Bonifacio, C. Pellegrini, L. M. Narducci Optics Communications **50**, 373 (1984)
[24] N. Sudar, P. Musumeci, J. Duris, Nucl. Inst. Meth. Phys. Res. A **865**, 39-42 (2017)
[25] C. Feng, D. Wang, Z. Zhao, "Pre-density modulation of the electron beam for soft x-ray FEL in the water window"
Proceedings of FEL 2010, Malmo, Sweden
[26] E. Hemsing, D. Xiang, Phys. Rev. ST Accel. Beams **16**, 010706 (2013)
[27] D. Cesar, et al., J. Appl. Phys. **118**, 234506 (2015)
[28] General Particle Tracer, http://www.pulsar.nl/gpt/.
[29] Radia, http://www.esrf.eu/Accelerators/Groups/InsertionDevices/So
[30] G. Andonian, et al., Appl. Phys. Lett. **98**, 202901 (2011)
[31] C. Emma et al., Appl. Phys. Lett. **110**, 154101 (2017)
[32] J. Duris et al., arXiv: 1704.05030v2
[33] C. Emma et al., "High efficiency tapered free-electron lasers with a pre-bunched electron beam"
Phys. Rev. Accel. Beams (To be published)